Fuel 274 (2020) 117877

Contents lists available at ScienceDirect

Fuel

journal homepage: www.elsevier.com/locate/fuel

Full Length Article

Determination of optical and dielectric properties of blends of alcohol with diesel and biodiesel fuels from terahertz spectroscopy

Magín Lapuerta[a,*], José Rodríguez-Fernández[a], Rayda Patiño-Camino[a], Alexis Cova-Bonillo[a], Esperanza Monedero[b], Yahya M. Meziani[c]

[a] Escuela Técnica Superior de Ingeniería Industrial, Universidad de Castilla-La Mancha, Edificio Politécnico, Avda. Camilo José Cela S-N, 13071 Ciudad Real, Spain
[b] Instituto de Investigación en Energías Renovables, Universidad de Castilla-La Mancha, 02006 Albacete, Spain
[c] NanoLab, Salamanca University, C/Espejo, 2, Edificio IDI, 37008 Salamanca, Spain

ARTICLE INFO

Keywords:
Alcohols
Biofuels
Dipole moment
Optical properties
Dielectric properties

ABSTRACT

The polarity and polarizability of fuel blend components determine some of the blend physical properties, such as viscosity, surface tension, fluidity or miscibility. This affects the development of the injected fuel jet and, therefore, the performance and pollutant formation in diesel engines. Among polar molecules, such as alcohols (ethanol and butanol), attractive forces exist between dipolar ends with opposite charges. The permanent molecular dipoles lead to the formation of induced dipoles in neighbouring molecules, which interact with the permanent dipoles forming intermolecular attraction. Although less appreciable, interaction between non-polar molecules also occurs in diesel fuels. In this study, the dielectric properties were investigated in the terahertz spectral region (located between infrared and microwaves). This region is typical for vibrational and rotational studies of molecules of non-conductive materials. For all blends tested, the time-domain terahertz spectra show that the amplitude of pulses decreases and the peak position shifts in time as alcohol content increases. For diesel and biodiesel fuels, amplitudes are higher and less delayed than for alcohols, indicating that they are less radiation-absorbing. The optical and dielectric properties (absorption coefficient, refraction index and dielectric constant) of alcohol blends with diesel and biodiesel blends were determined. For the alcohols studied, both absorption coefficient and refractive index decrease for increasing alkyl chain length. Real and imaginary terms of the complex dielectric function show increasing dependency with frequency as the molecule polarity increases. From these properties, the relaxation dynamics can be modelled for blends, and nonlinearities in their physical properties can be explained.

1. Introduction

The increasing problems of global warming, oil depletion, environmental pollution and the associated consequences, have promoted the use of alternative fuels. European Union has established increasingly restrictive target regarding the use of biofuels (up to 10% in 2020 [1] and to 14% in 2030 [2]) and at least 0.5% (2020) and 3.6% (2030) of this fraction will come from advanced biofuels, that is, from common waste, agricultural residues or non-food crops [3]. Among these, alcohols have been studied and applied in both gasoline and diesel engines with positives results in emissions and sustainability [4]. In particular, there is a large number of published studies [5–8] that describe the benefits of the use of ethanol and n-butanol in diesel blends [7], in biodiesel blends [9–11] or in diesel–biodiesel [12] blends.

The properties (viscosity, density, cold properties, etc.) of these blends have been adjusted to theoretical and empirical models based on interaction coefficients that highlight the importance of molecular interactions [13–15]. Such molecular interactions have not been clearly identified. The presence of alcohols (highly polar) in diesel fuel (mainly non-polar) causes the induced dipole–dipole Debye forces to manifest between a polar and non-polar molecule, which could explain such behaviours. In a natural way, the charge of a polar molecule causes a distortion in the electronic cloud of the non-polar molecule becoming transiently an induced dipole, generating mutual attraction. From the macroscopic standpoint this can be measured by means of the dielectric constant by applying controlled external electric fields. This is the principle of dielectric spectroscopy [16]. Khaled et al. [17] reviewed the dielectric properties of alcohols and their mixtures as biofuels, highlighting the complicated dielectric behaviour of alcohols.

Terahertz time-domain spectroscopy (THz-TDS) is a relatively

* Corresponding author.
E-mail address: magin.lapuerta@uclm.es (M. Lapuerta).

https://doi.org/10.1016/j.fuel.2020.117877
Received 12 February 2019; Received in revised form 11 April 2020; Accepted 14 April 2020
Available online 18 April 2020
0016-2361/

Nomenclature

Abbreviations and variables

A	Amplitude
B	Biodiesel
Bu	n-Butanol
CFPP	Cold Filter Plugging Point
D	Diesel fuel
d	Thickness of the sample
E	Electric field
Et	Ethanol
FAME	Fatty Acid Methyl Esters
FFT	Fast Fourier Transform
I	Intensity
LT-GaAs	Low-temperature gallium-arsenic photoconductive antennae
n	Refractive index
t	Time
TDS	Time-Domain Spectroscopy
THz	Terahertz
z	Volume fractions
θ	Phase
α	Absorption coefficient
k	Extinction coefficient
ω	Angular frequency

subscripts

exc	Excess
exp	Experimental
img	Imaginary part
j	Sample index
max	Maximum
real	Real part
ref	Reference

recent and developing spectroscopic technique, from which the materials are subjected to short pulses of terahertz radiation (with range covered from 0.1 to no more than 10 THz, approximately equivalent to 3–300 cm^{-1} or to 0.4–41.3 meV). THz radiation produces an alternating external electric field which interacts strongly with polar molecules but only very weakly with non-polar molecules, resulting in a differential radiation absorption according to the tested material composition. Such radiation-matter interaction is dominated by molecular interactions (van der Waals forces, London dispersion forces, etc.) but very particularly by hydrogen bonds. The result of THz-TDS is a terahertz's spectrum in which rotational and vibrational motions of polar and polarized molecules are manifested and further relaxed (dielectric relaxation) [18]. A major advantage of THz-TDS is that it allows the study of the interactions between the constituent molecules and the subsequent relaxation dynamics. This applies to inorganic and organic materials in gas, liquid, and solid phase.

The first studies published about the possibility of terahertz radiation for spectroscopy were reported by Smith et al. in 1988 [19], Fattinger & Grischkowsky in 1989 [20] and Siegel in 2002 [21]. Various studies have assessed the efficacy of THz-TDS and the number of publications concerning to its practical application has been growing in several fields of sciences: quality control in the food industry [22], exploration in the oil industry [23], imaging [24], pharmaceutical [25], biomedical [26], radioastronomy [27], sensing [28], etc. The use of this technique in the field of transport fuels is much more recent. Kim et al. [29] measured the refractive indices and absorption coefficient of gasoline, diesel, kerosene, and organic solvents, and binary mixtures between them, in the THz range (0.2–2.0 THz). They were able to identify the species in pure petroleum, products and organic solvents. From differences between the absorption spectra of biodiesel/diesel blends, De Sousa et al. [30] and Corach et al. [31] determined biodiesel content, or estimated the kinematic viscosity [32]. Expanding the work of Yomogida et al. [33] to higher frequencies, Sarkar et al. [34] analyzed the complex dielectric properties of a series of alcohols in 0.5–10.0 THz frequency range using THz-TDS. They highlighted that the characteristic peak of ethanol and n-butanol was registered at around 2 THz, which corresponds to hydrogen-type bonds. They were able to extend the range of study to molecules as small as the shortest alcohols. Arik et al. [35] measured the dielectric properties of diesel and gasoline samples using Terahertz spectroscopy on 0.1–1.1 THz frequency range. That same year, they published an article in which successfully characterized ethanol in gasoline samples on 0.2–1.6 THz frequency range [36]. They demonstrated the potential of this incipient technique for the study of complex mixtures, such as fuels. THz-TDS has been proposed as a quantitative technique, based on the correlation between some of the waveform features and the solute concentration [37–39]. These techniques, which are still under development, can provide accurate results, without requiring large amounts of sample.

In this work, the THz-time domain spectra of diesel, biodiesel, ethanol and n-butanol, together with ethanol–diesel, n-butanol-diesel, ethanol-biodiesel and n-butanol-biodiesel blends have been obtained from 0.2 to 1.1 THz, with the purpose to correlate their features with the type of base-fuel and alcohol and their concentrations. After the application of fast Fourier transforms (FFT), absorption coefficient and refractive index were obtained as a function of the frequency. From these properties, real and imaginary parts of dielectric function were obtained and analyzed with respect to the alcohol concentration of the blends. The information obtained suggests the possibility of a new method for the determination of alcohol content in blends, with the particularity of being nondestructive, safe for fuels (since this is a non-ionizing radiation), and requiring a small amount of sample. This information can be used to obtain the relaxation times characteristic of each alcohol in the blends by using the Debye model, or any other further-modified model. These relaxation times can be related to the macroscopic physical properties such as viscosity, miscibility, surface tension and cold flow properties, and therefore, can be useful to explain phenomena such as the fuel atomisation process in the combustion chamber. The data shown in this work also serves as an experimental support for comparison with data obtained by molecular dynamics simulation.

2. Material and methods

2.1. Materials

Diesel fuel was supplied by the Spanish company Repsol. The chemical composition by mass (obtained by high resolution mass spectrometry) consist of 30.66% paraffins, 44.61% naphtenes (resulting in 75% saturated) and 23.76% aromatics, without any oxygen content. This diesel fuel fulfils standard EN 590 [40]. Biodiesel fuel, produced from 80% soybean and 20% palm oils and fulfilling standard EN 14214 [41], was supplied by the Spanish company Bio Oils. The major composition by mass of biodiesel consists of 47.26% methyl linoleate (C18:2), 26.22% methyl oleate (C18:1), 15.626% methyl palmitate (C16:0), 5.39% methyl α-linolenate (C18:3) and 3.77% methyl stearate (C18:0), with methanol content below 0.15% (m/m). Henceforth, both diesel and biodiesel will be referred to as base-fuels. A more complete diesel and biodiesel composition is described in reference [14]. Two short chain monohydric alcohols were used for the preparation of the blends. Ethanol was donated by Abengoa Bioenergy and n-butanol was

supplied by Green Biologics Ltd. Table 1 shows the main properties of base-fuels and pure alcohols used for blends.

Samples were prepared for ethanol–diesel, n-butanol–diesel, ethanol–biodiesel and n-butanol–biodiesel pseudo-binary blends, with emphasis on low alcohol content blends due to the practical infeasibility of blends with high alcohol content in diesel engines. Therefore, samples were prepared at room temperature (around 25 °C) with 2.5, 5.0, 7.5, 10, 15, 20, 40, 60, 80 and 90% (v/v) of alcohol in base-fuel. In the case of ethanol/diesel blends, the test matrix was limited by the weak miscibility from 10% to 80% alcohol content at the working temperature [13]. For reference purposes, samples of neat diesel and biodiesel were also tested. Labelling of the samples was adopted from previous works [5,47]. For example, Et2.5-B indicates 2.5% (v/v) ethanol and 97.5% (v/v) biodiesel in the blended fuel.

2.2. Experimental setup

A schematic description of THz-time domain spectrometer (THz-TDS) is shown in Fig. 1. The instrument incorporates a femtosecond Ti:sapphire laser, which generates ultrashort pulses (60–80 fs) with 80 MHz frequency and around 650 mW average output power. Two low-temperature Gallium-Arsenic photoconductive antennae (LT-GaAs) were used for emission and detection of THz radiation. The emitted power of the THz radiation was around 10 μW. Silicon lenses were attached to the antennae for better efficiency. Aluminium coated parabolic mirrors were used to collimate the THz beam from the emitter through the sample to the detector. The sample cell was a 2 mm optical path quartz cuvette. The spectra were obtained in transmission mode. The signal was measured using the lock-in amplifier technique with high accuracy (error lower than 1 nV). More information of the system can be found in [48].

2.3. THz-TDS measurements

After switching on the laser, a time (approx. 30 min) was expected for the laser to reach thermal stability and at a working power of 0.670 W. The equipment was configured with a time step of 33.3 fs and N = 2048 points, obtaining an initial time window from −10 ps to 58.33 ps (further narrowed for analysis), with a total duration of 11 min per test. Before each test, the cuvette was flushed, cleaned with 2-propanol, dried with nitrogen, until it was free of stains and completely clean. In each case, a measurement of reference (empty cell) was taken. After the reference, the cuvette is filled with the sample by using a dropper ensuring that the sample covers the window above the focal point of the laser. Each complete test, with stable system operation, takes approximately 45 min. Measurements were taken at room conditions: 20 °C and 36% relative humidity, on average. This procedure was repeated for each sample and the data was collected for posterior treatment.

3. Results and discussion

3.1. THz spectroscopy results

Fig. 2 shows the resulting waveforms of the transmitted THz field for neat fuels, ethanol–diesel (Et-D), n-butanol-diesel (Bu-D), ethanol-biodiesel (Et-B) and n-butanol-biodiesel (Bu-D) blends at the concentrations previously described. The first graph in Fig. 2 (tagged neat fuels) shows the time-domain waveforms for the empty cell (used as reference), alcohols and base-fuels, and the following graphs show the waveforms corresponding to blends.

Two main differences between waveforms can be observed, both providing relevant information regarding the samples. The first is the difference in peak amplitudes (I_{max}). The attenuation of the peak intensity in the THz-TDS, indicates absorption by the sample with respect to that of the reference (empty cuvette) and can be quantified by Beer-Lambert's law. Among the fuels tested, ethanol is the most radiation-absorbing one and diesel is the least absorbing fuel. The second difference is between the peak positions or timings (t_{Imax}). This difference is related to the capacity of the sample to delay the radiation beam.

Table 1
Properties of fuels used for blends.

Property	Method	Diesel	Biodiesel	Ethanol	n-Butanol
This work tag-name		D	B	Et	Bu
Purity (%, v/v)		~	~	99.5	99.5
Density at 15 °C (kg/m^3)	EN ISO 3675	842.0	883.5	792.0	811.5
Kinematic viscosity at 40 °C (cSt)	EN ISO 3104	3.00	4.19	1.13	2.27
Lower heating value (MJ/kg)	UNE 51,123	42.93	37.64	26.84	33.20
C (wt %)		86.74	77.08	52.14	64.86
H (wt %)		13.26	11.91	13.13	13.51
O (wt %)		0	11.00	34.73	21.62
Water content (mg/kg)	EN ISO 12937	41.70	352.10	2024	1146
Molecular weight (kg/kmol)		208.20	291.26	46.07	74.12
H/C ratio		1.83	1.85	3	2.50
T10 (°C)	EN ISO 3405	188.5	338.4		
T50 (°C)	EN ISO 3405	274.0	339.7		
T95 (°C)	EN ISO 3405	346.9	345.8		
Boiling point (°C)[a]				78.37	117.4
Freezing Point (°C)[a]				−114.1	−89.8
CFPP (°C)	EN 116	−20	−1	< −51	< −51
Cloud Point (°C)	EN 23015	−4.1	2.1	< −120.7	−115.5
Pour Point (°C)	ASTM D97	−21	0	< −120.7	< −120.7
Lubricity (WS1.4) (μm)	EN ISO 12156-1	371	143	1057	571
Filterability	ASTM D2068	1.02	2.35	1.00	1.00
Derived Cetane number	EN 16715	52.65	52.48	8[b]	15.92
Refraction Index (at 590 nm)	ASTM D1218	1.458	1.452	1.356	1.397
Dipole moment (D)			1.68[c]	1.70[d]	1.66[d]
Mono/di/triglyceride content (% m/m)	EN 14105		0.26/0.10/0.05		
Free/total glycerol content (% m/m)	EN 14105		0.009/0.096		

a: taken from Poling et al. [42].
b: taken from Zelenka et al. [43] and Xiaolu et al. [44].
c: calculated from second-order contribution group method proposed by Müller et al. [45].
d: obtained from www.trimen.pl [46].

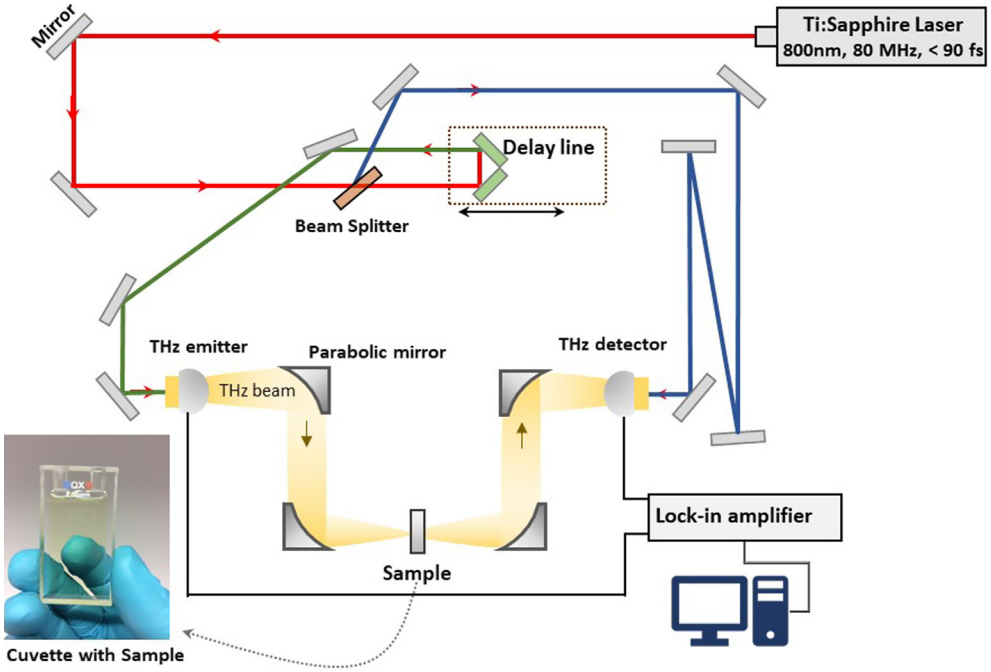

Fig. 1. Layout of the terahertz time domain spectroscopy system (THz-TDS).

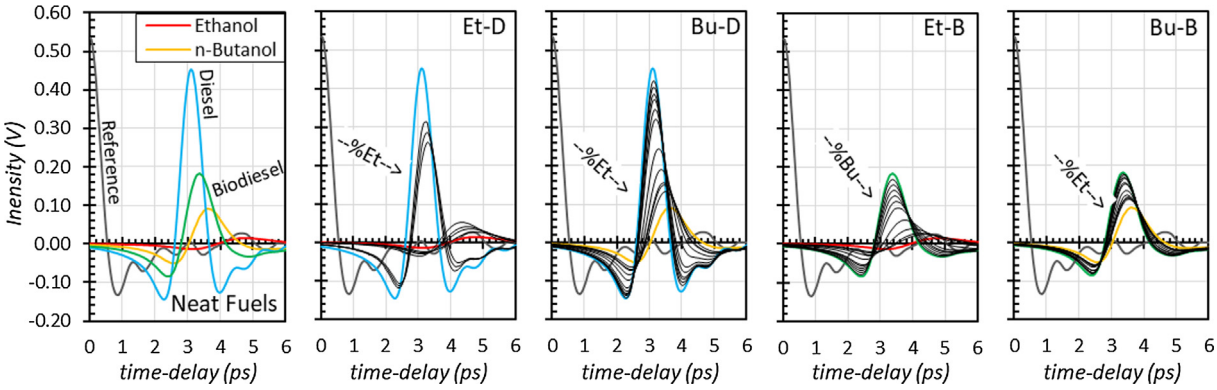

Fig. 2. Transmitted THz waveforms obtained with a 2.0 mm cuvette for neat fuels and ethanol–diesel (Et-D), ethanol-biodiesel (Et-B), n-butanol-diesel (Bu-D) and n-butanol-biodiesel (Bu-B) blends at different concentrations.

Thus, if the sample has higher polarity (like alcohols), it slows down the radiation speed, thus its peak appears later than any sample with lower polarity (like diesel). The order of the peak intensities correlates with order in energy absorption and the order in peak timing correlates with polarity. Both orders are ethanol > n-butanol > biodiesel > diesel, as expected. It should be remarked that refractive indexes shown in Table 1 correspond to very high frequencies ($\lambda \approx 590$ nm) and therefore, no correlation should be expected with the peak timing in the THz domain. From results for blends (Et-D, Bu-D, Et-B and Bu-B), the first obvious observation is that the blend pulses lie between those corresponding to their neat components, both in I_{max} and t_{Imax}. A practical implication of this is the possibility of determining blend concentrations using THz-TDS.

To get further insight, the maximum amplitude for each peak, I_{max}, and the corresponding time, t_{Imax}, are shown in Fig. 3 against the alcohol percentage in volume in diesel blends (solid lines, with dashed sector for the immiscible range) and biodiesel blends (dotted lines). According to Fig. 3 (right), a linear correlation between t_{Imax} and alcohol concentration (% v/v) can be extracted. At very low or very high alcohol concentration some nonlinearities can be observed. In all cases, the slope of linearity is proportional to the difference in polarity between the blend components. The straight line with highest slope corresponds to Et-D blends, which implies the best sensitivity either for determination of the blend concentration or for modelling dielectric properties. On the contrary, the line corresponding to Bu-B blends, both components with medium polarity, is the least sensitive. For example,

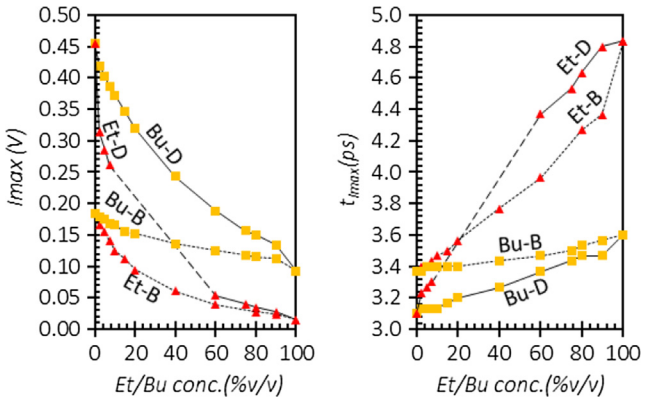

Fig. 3. Effect of the alcohol concentration (%v/v) on I_{max} (left) and t_{Imax} (right).

for the current system configuration, the limited resolution of a detection method would not distinguish between Bu2.5-B and Bu20-B. Anyhow, the resolution could be improved by using a wider cuvette.

3.2. Results derived from the Fourier transform of THz spectra

Each spectrum was preprocessed to smooth it and only the first peak was selected. Zero padding technique was applied from the pulse end to 40 ps. Spectra treatment was based on the conceptual framework proposed by Zhang et al. [49] and used by other researchers [31–33]. The distribution of the THz pulse in the frequency domain, $E(\omega)$, is related to the temporal waveform $E(t)$ according to:

$$E(\omega) = A(\omega)\cdot e^{-i\cdot\theta(\omega)} = \int E(t)\cdot e^{-i\cdot\omega\cdot t}\cdot dt \quad (1)$$

By applying fast Fourier transform (FFT) to a temporal waveform ($E(t)$), amplitude $A(\omega)$ and phase $\theta(\omega)$ were obtained as a function of angular frequency (ω). This was done by using OriginPro [50]. Fresnel's equations relate the radiation transmitted through a sample and its optical constants, absorption coefficient $\alpha(\omega)$ and the real part of the refractive index $n(\omega)$:

$$\alpha(\omega)_j = -\frac{2}{d}\ln\left[\frac{A(\omega)_j}{A(\omega)_{ref}}\right] \quad (2)$$

$$n(\omega)_j = n_{ref} + [\theta(\omega)_j - \theta(\omega)_{ref}]\cdot\frac{c}{\omega\cdot d} \quad (3)$$

where j is any sample signal waveform, *ref* is the reference signal, d is the thickness of the sample (2.0 mm) and c is the speed of light in vacuum ($2.998\cdot10^8$ m/s). In all cases, a waveform obtained with the empty cuvette was used as the reference signal, so n_{ref} is taken as 1. Power transmission, absorption coefficient and refractive index, all of these as a function of f (in THz) are shown in Fig. 4 for all samples in the same order as Fig. 4 (neat fuels, Et-D, Bu-D, Et-B and Bu-D).

As shown in Fig. 4, the four power spectra exhibit similar patterns. As expected, in each case, the spectrum moves monotonically from the base-fuel to the corresponding alcohol as the alcohol concentration increases. It should be noted that no spectra appear in the intermediate concentration range (from 10 to 60%) for ethanol/diesel blends as a consequence of the non-miscibility of these blends. This is necessarily replicated in the graphs for the other derived properties.

Besides the fluctuations of the technique itself [51] (despite the application of smoothing processes before applying FFT), additional peaks can be observed as a consequence of water absorption (0.558, 0.753, 0.989, 1.099, 1.15 THz), which is another source of uncertainty. These peaks are evident in the power spectra of ethanol and high ethanol content blends, and to a lesser degree in the low ethanol content blends. This is due the presence of humidity in the neat ethanol. H-bonding from the hydroxyl group makes ethanol highly hygroscopic. n-butanol also shows moisture traces but with much weaker intensity as it

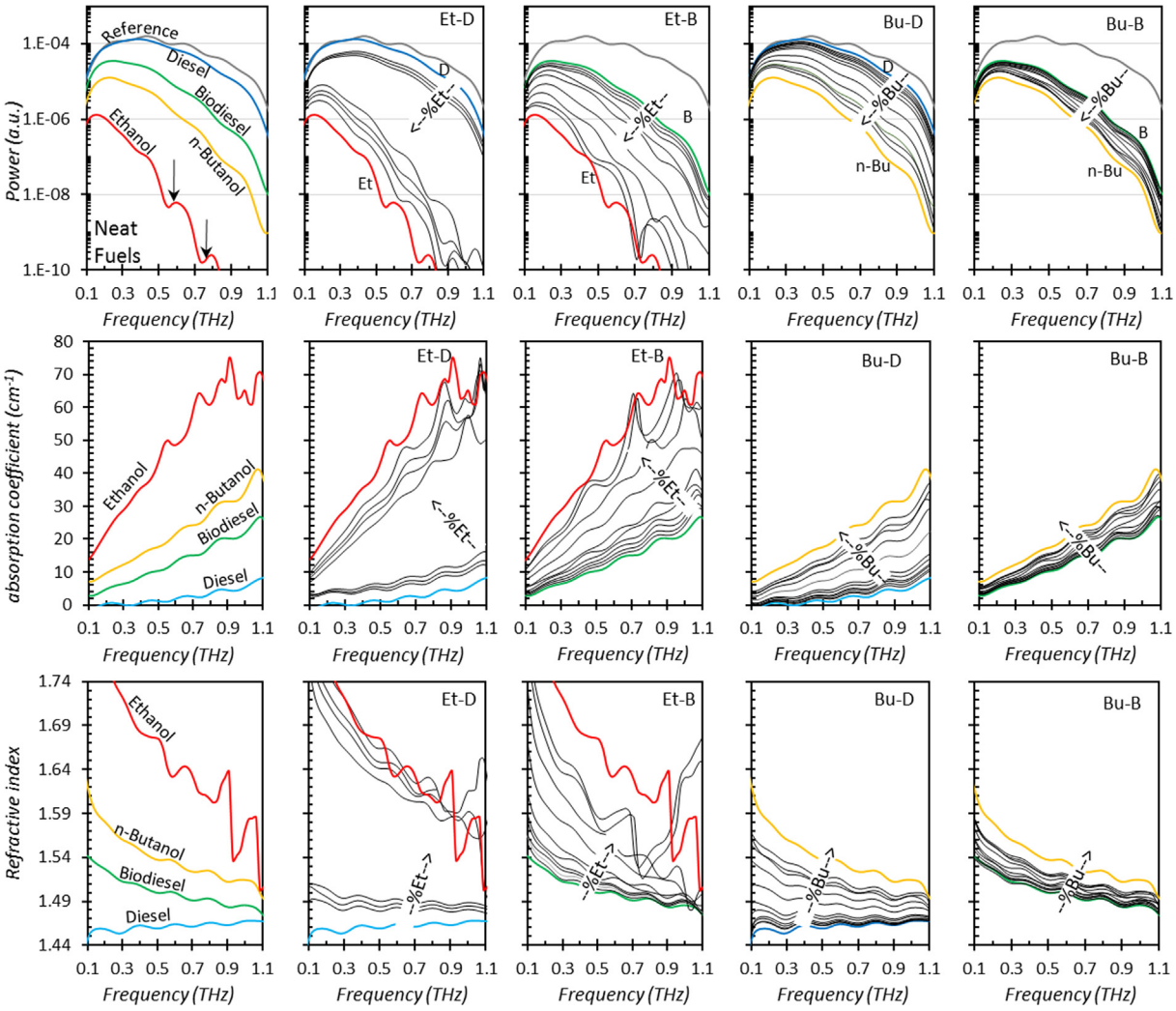

Fig. 4. Power absorption spectrum (top), absorption coefficient (center) and refractive index (bottom) of ethanol–diesel (Et-D), ethanol-biodiesel (Et-B), n-butanol-diesel (Bu-D) and n-butanol-biodiesel (Bu-B) blends at different concentrations after Fourier transform.

is less hygroscopic. This effect is replicated in all derived parameters for these fuels. Another implication of this is the possibility to use THz-TDS to identify water contamination on like-diesel fuels. In all cases, the order in which the spectra for the different blends are shown is consistent with the alcohol content.

Fig. 4 (central row) shows the absorption coefficient spectra of samples as a function of frequency, $\alpha(\omega)_j$, ranging from 0 to 80 cm^{-1} across the 0.1–1.1 THz range, which are consistent with spectra shown by other authors for gasoline, diesel and alcohols [34–36]. Ethanol has a much higher absorbance compared to n-butanol [34] and to all other fuels throughout the entire studied broadband, consistently with its highest polarity. For all neat fuels, the absorption coefficients increase with the increase in frequency, and such increase follows the same order previously described. There is also a higher increase in biodiesel absorption coefficient compared to diesel, whose increase in absorption coefficient is basically marginal within the frequency range studied. For blends, the absorption coefficient increases consistently with increasing alcohol content. The results are similar to those reported for ethanol-gasoline blends by Arik et al. [36].

To analyse the effect of blending components on the properties of the blend, the experimental absorption coefficient is compared to that calculated based on the contribution of its components. Using thermodynamic nomenclature, the excess absorption coefficient can be defined. This is the opposite of the relative absorption coefficient used in other works [52,53]. The excess absorption coefficient, $\alpha_{exc}(\omega)$, was defined as the difference between the experimental absorption coefficients, $\alpha_{exp}(\omega)$, and the ideal ones, and was calculated using Eq. (4):

$$\alpha_{exc}(\omega) = \alpha_{exp}(\omega) - \sum_{i}^{n} z_i \alpha(\omega)_i \tag{4}$$

where z_i are the volume fractions and i are the blend components. The results obtained for excess absorption coefficient are presented in Fig. 5. These were obtained without further processing of the data to eliminate the effects of moisture on ethanol and its blends. The resulting spectra show significant instabilities, magnified by the scale used, which may hinder the observation of clear trends. Although a strong nonideal (excess different to zero) and unstable (oscillating) behavior is evident for all blends, when comparing ethanol with n-butanol blends, the former introduces higher nonideality to the blends. This is explained because polarizability between ethanol and the base-fuels is higher than that of n-butanol (in addition to the effect of moisture mentioned above). The instabilities in biodiesel blends (with both alcohols) are more pronounced than with diesel. In this case, both fuels are polarizable, which may lead to synergistic interactions.

At low alcohol contents, α_{exc} is positive because alcohol molecules are more free to rotate and consequently to absorb energy than when they are surrounded by larger amounts of alcohol molecules. This effect is less pronounced with biodiesel (which has some polarity) because

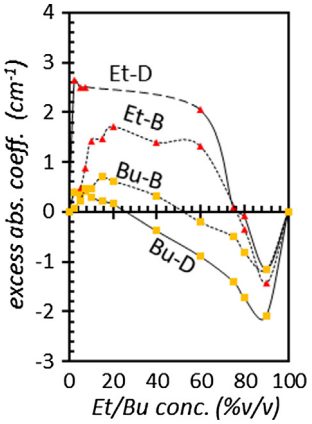

Fig. 6. Excess absorption coefficient of ethanol–diesel (Et-D), ethanol-biodiesel (Et-B), n-butanol-diesel (Bu-D) and n-butanol-biodiesel (Bu-B) blends. α_{exc} was averaged over 0.2 to 1.1 THz frequency range.

biodiesel/alcohol interactions, where hydrogen bonds can be formed between hydroxyl and carboxylic groups. The narrow difference between α_{exc} from Et2.5-D to Et7.5-D, and the slight variation with frequency, suggests that the absorption is controlled by diesel fuel. At the other extreme, at high alcohol concentrations (or low diesel concentrations), the excess absorption is negative, because alcohol molecules are replaced by diesel molecules which disturb the hydrogen bond network between alcohol molecules and replace them by weaker London and Van der Walls interactions, and a slower rotational dynamics. The results of averaging the excess absorption coefficient over the entire frequency bandwidth are presented in Fig. 6 for all blends.

As in the case of the absorption coefficient spectra, the decreasing rate of the refractive index spectra for neat fuels (Fig. 4 bottom) is consistent with the polarizability of fuels. In the range studied (frequencies below 1.1 THz) the refractive indices of alcohols are higher and have higher decreasing rates with frequency, while those of base-fuel are lower. This order is contrary to the order obtained at 590 nm (Table 1), but it is expected that at very high frequencies, the order will match with that displayed in Table 1, as shown by Sakar et al. [34].

3.3. Complex dielectric function

The dynamic behavior of the liquids can be quantified with the complex dielectric function, also called relative permittivity. Previously, the extinction coefficient, $k(\omega)$, must be calculated. Both are based on $\alpha(\omega)$ and $n(\omega)$, defined above:

$$k(\omega) = \frac{c \cdot \alpha(\omega)}{2 \cdot \omega} \tag{5}$$

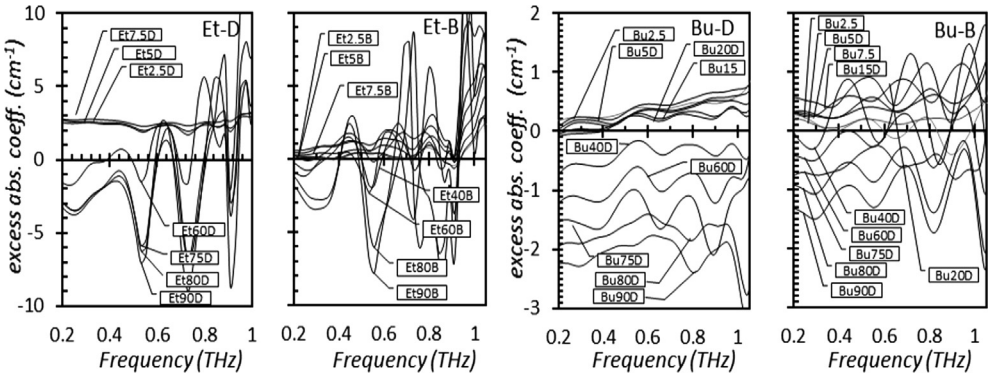

Fig. 5. Excess absorption coefficient of ethanol–diesel (Et-D), ethanol-biodiesel (Et-B), n-butanol-diesel (Bu-D) and n-butanol-biodiesel (Bu-B) blends. Et-D/ Et-B and Bu-D/Bu-B share the ordinate axis.

$$\varepsilon(\omega) = [n^2(\omega) - k^2(\omega)] + i[2n(\omega)\cdot k(\omega)] \quad (6)$$

Fig. 7 shows the frequency and alcohol concentration dependences for both real (top) and imaginary (bottom) terms of the complex dielectric function $\varepsilon(\omega)$ for diesel and biodiesel blends. The real part, $\varepsilon_{real}(\omega)$, is proportional to the energy-storage capacity, while the imaginary part, $\varepsilon_{img}(\omega)$, also known as loss factor, represents the loss of energy that the electric dipoles present by friction effects (mainly by rotational effects) when trying to align with the changing direction of the electric field. The higher the imaginary term, the higher the energy dissipated from these movements. A high dependence on frequency can be observed, especially for alcohols, (red for ethanol, orange for n-butanol). Both real and imaginary terms show similar patterns: both decrease as the frequency increases, indicating dominance of OH group polarization. This decreasing effect is more pronounced for ethanol than for n-butanol, consistently with the higher polarizability of ethanol with respect to n-butanol, with longer carbon chain which weakens the polarization induced by the external radiation in the presence of the OH group, as demonstrated in previous studies about monohydric alcohols [33,34].

For diesel (blue) and biodiesel (green) fuels, the effect of frequency is much less important than for alcohols. Diesel fuel shows a real term of the dielectric function practically invariable ($\approx$2.1) with frequency and an imaginary term almost zero. This indicates that diesel fuel, besides being composed by basically non polar molecules, is also basically non polarizable. These results are consistent with that from Arik et al. [35]. A slight increase is observed for biodiesel with respect to diesel fuel, which is associated with carboxyl groups of FAME, which can be polarized in the presence of an external radiation. However, these molecules are complemented with carbon chains from 12 to 24 -CH_2- groups, which not only substantially reduce their polarity but also their polarizability.

4. Conclusions

The present study was aimed to determine the effect of ethanol and n-butanol content on the optical and dielectric properties of diesel and biodiesel blends. The following conclusions can be drawn:

- The order of appearance of the pulses in the time domain corresponding to the neat fuels coincides with their degree of polarity. While amplitude increases with the carbon chain length, time shift decreases. For diesel and biodiesel fuels, amplitudes are higher and are less delayed than for alcohols, indicating that they are less radiation-absorbing.
- For all blends, the time-domain pulses show that the amplitude decreases and the peak position shifts in time as alcohol concentration increases.
- For the studied alcohols, both absorption coefficient and refractive index decrease as the alkyl chain length increases. For neat fuels and its blends, the refractive index decreases asymptotically as the frequency increases from 0.1 THz to 1.1 THz.
- Real and imaginary terms of the complex dielectric function show similar patterns, with increasing dependency with frequency as the molecule polarity increases, indicating that for the fuels and blends studied, polarizability increases with polarity.

For low alcohol contents (less than 10%) using a cuvette with a larger optical path is recommended, since it would provide more detailed information in the range of alcohol contents of practical application. From the spectral results shown here, further modelling work has to be conducted in order to adjust the dielectric behavior of the blends to the most suitable dynamic relaxation model. Based on the literature, Debye's model seems to be the most appropriate, but the number of relaxation processes differs for the different fuels used here, which implies a challenge, especially for modelling blends. In any case, the relaxation times provide information to interpret the interaction forces between components of the blends and to explain their nonlinear macroscopic properties.

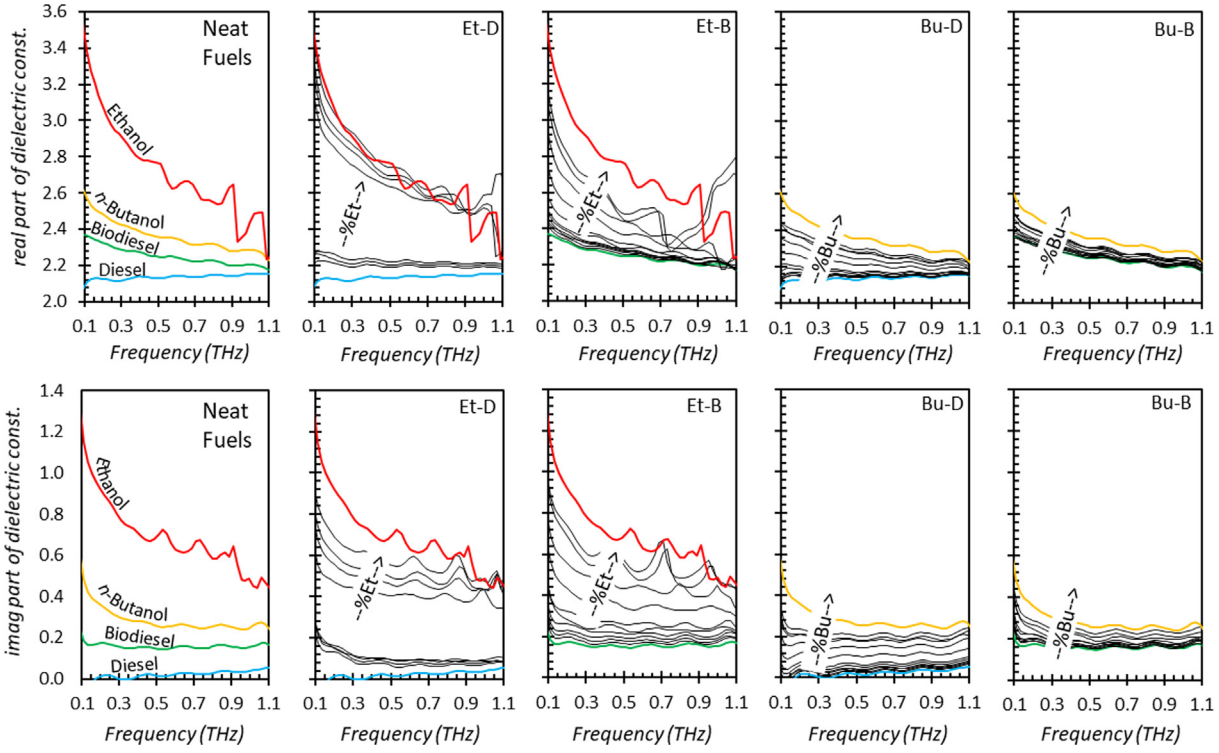

Fig. 7. Real (top) and imaginary (bottom) terms of dielectric constant of ethanol–diesel (Et-D), ethanol-biodiesel (Et-B), n-butanol-diesel (Bu-D) and n-butanol-biodiesel (Bu-B) blends.

CRediT authorship contribution statement

Magín Lapuerta: Conceptualization, Methodology, Supervision, Writing - review & editing. **José Rodríguez-Fernández:** Methodology, Supervision, Writing - review & editing. **Rayda Patiño-Camino:** Visualization, Investigation, Data curation, Writing - original draft. **Alexis Cova-Bonillo:** Investigation, Data curation, Writing - original draft. **Esperanza Monedero:** Formal analysis, Visualization. **Yahya M. Meziani:** Methodology, Investigation, Resources.

Declaration of Competing Interest

The authors declare that they have no known competing financial interests or personal relationships that could have appeared to influence the work reported in this paper.

Acknowledgements

Repsol, Bio Oils, Abengoa Bioenergy and Green Biologics are gratefully acknowledged for the donation of diesel fuel, biodiesel fuel, ethanol and n-butanol, respectively.

References

[1] Directive 2009/28/EC. The promotion of the use of energy from renewable sources and amending and subsequently repealing, Off J EU, L 140, 16–62, 2009.
[2] Revised Renewable Energy Directive. https://ec.europa.eu /energy/sites/ener/files/ documents/.
[3] Directive 2015/1513/EC. The quality of petrol and diesel fuels and amending, Off J EU, L 239, 1–29, 2009.
[4] Celebi Y, Aydin H. An overview on the light alcohol fuels in diesel engines. Fuel 2019;236:890–911. https://doi.org/10.1016/j.fuel.2018.08.138.
[5] Lapuerta M, Hernandez J, Fernandez-Rodriguez D, Cova-Bonillo A. Autoignition of blends of n-butanol and ethanol with diesel or biodiesel fuels in a constant-volume combustion chamber. Energy 2017;118(1):613–21. https://doi.org/10.1016/j.energy.2016.10.090.
[6] Kumar S, Hyun Cho J, Park J. Advances in diesel–alcohol blends and their effects on the performance and emissions of diesel engines. Renew Sustain Energy Rev 2013;22:46–72. https://doi.org/10.1016/j.rser.2013.01.017.
[7] Giakoumis E, Rakopoulos C, Dimaratos A, Rakopoulos D. Exhaust emissions with ethanol or n-butanol diesel fuel blends during transient operation: a review. Renew Sustain Energy Rev 2013;17:170–90. https://doi.org/10.1016/j.rser.2012.09.017.
[8] Jamrozik A, Tutak W, Pyrc M, Gruca M, Kočiško M. Study on co-combustion of diesel fuel with oxygenated alcohols in a compression ignition dual-fuel engine. Fuel 2018;221:329–45. https://doi.org/10.1016/j.fuel.2018.02.098.
[9] Wei L, Cheung C, Ning Z. Effects of biodiesel-ethanol and biodiesel-butanol blends on the combustion, performance and emissions of a diesel engine. Energy 2018;155:957–70. https://doi.org/10.1016/j.energy.2018.05.049.
[10] Zheng Z, Xia M, Liu H, Yao M. Experimental study on combustion and emissions of dual fuel RCCI mode fueled with biodiesel/n-butanol, biodiesel/2,5-dimethylfuran and biodiesel/ethanol. Energy 2018;148:824–38. https://doi.org/10.1016/j.energy.2018.02.015.
[11] Kuszewski H. Experimental investigation of the autoignition properties of ethanol–biodiesel fuel blends. Fuel 2019;235:1301–8. https://doi.org/10.1016/j.fuel.2018.08.146.
[12] Mehta R, Chakraborty M, Mahanta P, Parikh P. Evaluation of fuel properties of butanol-biodiesel-diesel blends and their impact on engine performance and emissions. Ind Eng Chem Res 2010;49:7660–5https://pubs.acs.org/doi/abs/10.1021/ie1006257.
[13] Lapuerta M, García-Contreras R, Campos-Fernández J, Dorado MP. Stability, lubricity, viscosity, and cold-flow properties of alcohol-diesel blends. Energy Fuels 2010;24:4497–502https://pubs.acs.org/doi/abs/10.1021/ef100498u.
[14] Lapuerta M, Rodríguez-Fernández J, Fernández-Rodríguez D, Patiño-Camino R. Cold flow and filterability properties of n-butanol and ethanol blends with diesel and biodiesel fuels. Fuel 2018;224(15):552–9. https://doi.org/10.1016/j.fuel.2018.03.083.
[15] Lapuerta M, Rodríguez-Fernández J, Fernández-Rodríguez D, Patiño-Camino R. Modeling viscosity of butanol and ethanol blends with diesel and biodiesel fuels. Fuel 2017;199:332–8.
[16] Kremer F, Schönhals A. Broadband dielectric spectroscopy. Berlin, Heidelberg: Springer; 2003.
[17] El Khaled D, Novas N, Gázquez J, García R, Manzano-Agugliaro F. Alcohols and alcohols mixtures as liquid biofuels: a review of dielectric properties. Renew Sustain Energy 2016;66:556–71. https://doi.org/10.1016/j.rser.2016.08.032.
[18] Oka A, Tominaga K. Terahertz spectroscopy of polar solute molecules in non-polar solvents. J Non-Cryst Solids 2006;352(42–49):4606–9. https://doi.org/10.1016/j.jnoncrysol.2006.03.122.
[19] Smith P, Auston D, Nuss M. Subpicosecond photoconducting dipole antennas. IEEE J Quantum Electron 1988;24(2):255–60. https://doi.org/10.1109/101.485909.
[20] Fattinger C, Grischkowsky D. Terahertz beams. Appl Phys Lett 1989;54(490):490–2. https://doi.org/10.1063/1.100958.
[21] Siegel P. Terahertz technology. IEEE Trans Microw Theory Tech 2002;50(3):910–28. https://doi.org/10.1109/22.989974.
[22] Gowen A, O'sullivan C, O'donnella C. Terahertz time domain spectroscopy and imaging: Emerging techniques for food process monitoring and quality control. Trends Food Sci Technol 2012;25(1):40–6. https://doi.org/10.1016/j.tifs.2011.12.006.
[23] Zhan H, Chen M, Zhao K, Li Y, Miao X, Ye H, et al. The mechanism of the terahertz spectroscopy for oil shale detection. Energy 2018;161:46–51. https://doi.org/10.1016/j.energy.2018.07.112.
[24] Wallace H. Analysis of RF imaging applications at frequencies over 100 GHz. Appl Opt 2010;49(19):E38–47. https://doi.org/10.1364/AO.49.000E38.
[25] Shen Y. Terahertz pulsed spectroscopy and imaging for pharmaceutical applications: a review. Int J Pharm 2011;417(1–2):48–60. https://doi.org/10.1016/j.ijpharm.2011.01.012.
[26] Yang X, Zhao X, Yang K, Liu Y, Liu Y, Fu W, et al. Biomedical applications of terahertz spectroscopy and imaging. Trends Biotechnol 2016;34:810–24. https://doi.org/10.1016/j.tibtech.2016.04.008.
[27] Graf U, Honingh C, Jacobs K, Stutzki J. Terahertz heterodyne array receivers for astronomy. J Infrared Milli Terahz Waves 2015;36:896–921. https://doi.org/10.1007/s10762-015-0171-7.
[28] Sinha A, Dhanjai, Zhao H, Huang Y, Lu X, Chen J, Jain R. MXene: an emerging material for sensing and biosensing. Trends Anal Chem 2018;105:424–35. https://doi.org/10.1016/j.trac.2018.05.021.
[29] Kim G, Jeon S, Kim J, Jin Y. Terahertz time domain spectroscopy of petroleum products and organic solvents, de 33rd International Conference on Infrared, Millimeter and Terahertz Waves 2008; Pasadena, CA, USA. https://doi.org/10.1109/ICIMW.2008.4665664.
[30] De Souza JE, Scherer MD, Cáceres JAS, Caires ARL, M'Peko JC. A close dielectric spectroscopic analysis of diesel/biodiesel blends and potential dielectric approaches for biodiesel content assessment. Fuel 2013;105:705–10. https://doi.org/10.1016/j.fuel.2012.09.032.
[31] Corach J, Sorichetti PA, Romano SD. Permittivity of biodiesel-rich blends with fossil diesel fuel: application to biodiesel content estimation. Fuel 2016;177:268–73. https://doi.org/10.1016/j.fuel.2016.02.086.
[32] Corach J, Colman M, Sorichetti PA, Romano SD. Kinematic viscosity of soybean biodiesel and diesel fossil fuel blends: Estimation from permittivity and temperature. Fuel 2017;207:488–92. https://doi.org/10.1016/j.fuel.2017.06.102.
[33] Yomogida Y, Sato Y, Nozaki R, Mishina T, Nakahara J. Dielectric study of normal alcohols with THz time-domain spectroscopy. J Mol Liq 2010;154:31–5. https://doi.org/10.1016/j.molliq.2010.03.007.
[34] Sarkar S, Saha D, Banerjee S, Mukherjee A, Mandal P. Broadband terahertz dielectric spectroscopy of alcohols. Chem Phys Lett 2017;678:65–71. https://doi.org/10.1016/j.cplett.2017.04.026.
[35] Arik E, Altan H, Esenturk O. Dielectric properties of diesel and gasoline by terahertz spectroscopy. J Infrared Millimeter Terahertz Waves 2014;35(9):759–69. https://doi.org/10.1007/s10762-014-0081-0.
[36] Arik E, Altan H, Esenturk O. Dielectric properties of ethanol and gasoline mixtures by terahertz spectroscopy and an effective method for determination of ethanol content of gasoline. J Phys Chem A 2014; n°;118:3081–9.
[37] Matoug M, Gordon R. Crude oil asphaltenes studied by terahertz spectroscopy. 3. ACS Omega; 2018. p. 3406–12. https://pubs.acs.org/doi/pdf/10.1021/acsomega.8b00017.
[38] Heyden M, Bründermann E, Heugen U, Niehues G, Leitner D, Havenith M. Long-range influence of carbohydrates on the solvation dynamics of water–answers from terahertz absorption measurements and molecular modeling simulations. J Am Chem Soc 2008;130(17):5773–9https://pubs.acs.org/doi/abs/10.1021/ja0781083.
[39] Song Y, Zhan H, Zhao K, Miao X, Lu Z, Bao R, et al. Simultaneous characterization of water content and distribution in high-water-cut crude oil. Energy Fuels 2016;30:3929–33. https://doi.org/10.1021/acs.energyfuels.6b00340.
[40] EN 590. Automotive fuels-Diesel-Requirements and test methods. European Committee for Standarization, Brussels, Belgium, 2017.
[41] EN 14214. Automotive fuels. Fatty acid methyl esters (FAME) for diesel engines, European Committee for Standarization, Brussels, Belgium, 2018.
[42] Poling E, Praunitz J, O'Connell J. The properties of gases and liquids. fourth ed. New York: McGraw-Hill; 2000.
[43] Zelenka P, Kapus P, Mikulic L. Development and optimization of methanol fueled compression ignition engines for passenger cars and light duty trucks, SAE Technical Paper 1991; n° 910851. https://doi.org/10.4271/910851.
[44] Xiaolu L, Xinqi Q, Liang Z, Junhua F, Zhen H, Huimin X. Combustion and emission characteristics of a two-stroke diesel engine operating on alcohol. Renew Energy 2005;30(13):2075–84. https://doi.org/10.1016/j.renene.2004.05.014.
[45] Müller K, Mokrushina L, Arlt W. Second-order group contribution method for the dipole moment. J Chem Eng Data 2012;57:1231–6https://pubs.acs.org/doi/pdf/10.1021/je2013395.
[46] Trimen Chemicals. http://www.trimen.pl/witek/ciecze/old_liquids.html; [accessed: 10 January 2020].
[47] Hernández J, Lapuerta M, Cova-Bonillo A. Autoignition reactivity of blends of diesel and biodiesel fuels with butanol isomers. J Energy Inst 2018:1–9. https://doi.org/10.1016/j.joei.2018.05.008.
[48] García-García E, Diez E, Meziani Y, Velázquez-Pérez J, Calvo-Gallcao J. Terahertz time domain spectroscopy for chemical identification, Spanish Conference on Electron Devices, Valladolid, Spain, 2013. DOI: https://doi.org/10.1109/CDE.2013.6481377.

[49] Zhang X, Xu J. Introduction to THz wave photonics. first ed. New York: Springer; 2010. 2018.
[50] Corporation OriginLab. OriginLab 2018. MA: Northampton; 2018.
[51] Ji T, Zhang Z, Zhao H, Chen M, Yu X, Xiao T. A THz-TDS measurement method for multiple samples. Opt Commun 2014;312:292–5. https://doi.org/10.1016/j.optcom.2013.09.013.
[52] Li R, Dagostino C, Mcgregor J, Mantle M, Zeitler J, Gladden L. Mesoscopic structuring and dynamics of alcohol/water solutions probed by terahertz time-domain spectroscopy and pulsed field gradient nuclear magnetic resonance. J Phys Chem B 2014;118:10156–66. https://doi.org/10.1021/jp502799x.
[53] Tassaing T, Danten Y, Besnard M, Zoïdis E, Yarwood J. A far infrared study of benzene-fluorinated benzene binary. mixturesChem Phys 1994;184(1–3):225–31. https://doi.org/10.1016/0301-0104(94)00106-5.